Frontiers of Information Technology & Electronic Engineering
www.jzus.zju.edu.cn; engineering.cae.cn; www.springerlink.com
ISSN 2095-9184 (print); ISSN 2095-9230 (online)
E-mail: jzus@zju.edu.cn

Modified dynamic event-triggered scaled formation control for multi-agent systems via a sparrow search algorithm based co-design algorithm*

Yanping YANG[1,2], Siyu MA[1,2], Dawei LI‡[1,2,3], Jinghui SUO[1,2]

[1]*College of Information Science and Technology, Donghua University, Shanghai 201620, China*

[2]*Engineering Research Center of Digitized Textile & Apparel Technology, Donghua University, Shanghai 201620, China*

[3]*State Key Laboratory for Modification of Chemical Fibers and Polymer Materials, College of Information Science and Technology, Donghua University, Shanghai 201620, China*

E-mail: yangyanping@dhu.edu.cn; smithereens_msy@163.com; ldwei1986@163.com; suojinghui@dhu.edu.cn

Received Sept. 9, 2023; Revision accepted Dec. 10, 2023; Crosschecked Jan. 12, 2024

Abstract: This paper is concerned with the scaled formation control problem for multi-agent systems (MASs) over fixed and switching topologies. First, a modified resilient dynamic event-triggered (DET) mechanism involving an auxiliary dynamic variable (ADV) based on sampled data is proposed. In the proposed DET mechanism, a random variable obeying the Bernoulli distribution is introduced to express the idle and busy situations of communication networks. Meanwhile, the operation of absolute value is introduced into the triggering condition to effectively reduce the formation error. Second, a scaled formation control protocol with the proposed resilient DET mechanism is designed over fixed and switching topologies. The scaled formation error system is modeled as a time-varying delay system. Then, several sufficient stability criteria are derived by constructing appropriate Lyapunov–Krasovskii functionals (LKFs). A co-design algorithm based on the sparrow search algorithm (SSA) is presented to design the control gains and triggering parameters jointly. Finally, numerical simulations of multiple unmanned aerial vehicles (UAVs) are presented to validate the designed control method.

Key words: Scaled consensus; Formation control; Dynamic event-triggered scheme; Switching topology
https://doi.org/10.1631/FITEE.2300615 **CLC number:** TP13

1 Introduction

With the recent advances in network communication engineering and automatic control technologies, the cooperative control for multi-agent systems (MASs) has attracted ever growing attention because of its wide application scopes in various fields, such as microgrids (Shan et al., 2021; Ning et al., 2023), multi-vehicle systems (Ge et al., 2022, 2023; Xie et al., 2023; Zhang XM et al., 2023), wireless sensor networks (Guan and Ge, 2018; Ge et al., 2019; Shen et al., 2020), and distributed games (Ye MJ et al., 2023). Specifically, an MAS is usually composed of a mass of distributed agents interconnected through some network medium. Through mutual information exchange and interaction between individuals, MASs can accomplish a large number of complicated tasks that are beyond the capabilities of individual agents (He et al., 2022; Su et al., 2022). The agents in MASs can eventually achieve cooperative goals through collaborative control strategies like rendezvous, target encirclement, formation control, and consensus control (Cao et al., 2013).

‡ Corresponding author

* Project supported by the National Natural Science Foundation of China (Nos. 62103097 and 61803081), the Shanghai Rising-Star Program (No. 21QA1400100), and the Natural Science Foundation of Shanghai, China (No. 20ZR1400800)

ORCID: Yanping YANG, https://orcid.org/0000-0001-6900-7241; Dawei LI, https://orcid.org/0000-0002-9702-8848

In the past years, consensus control has been studied thoroughly in the context of collaborative control of MASs. In common consensus control issues, all agents in an MAS eventually reach the same state. Zhang D et al. (2018) proposed an alternative switched system model to address the consensus problem in heterogeneous linear MASs with nonuniform sampling. Hu et al. (2019) explored the consensus control of high-order MASs with antagonistic interactions and communication noises, where a control strategy employing random approximation was devised by leveraging the information from neighboring agents. Chen et al. (2022) solved the path-following control problem for MASs within finite time. Zhang LZ et al. (2022) investigated the bipartite asynchronous impulsive tracking consensus control for MASs with nonzero leader control inputs. However, in some scenarios, consensus is insufficient to handle complex environments. For example, when aircrafts are searching for targets, the positions of the targets can be determined more efficiently through reasonable formation flights. Therefore, formation control, owing to its practical applications, has widely been an area of interest recently. Yu JL et al. (2022) discussed the adaptive optimal time-varying formation tracking control for MASs having a noncooperative leader, and this was achieved in their research through the design of a new formation tracking protocol involving extended state observers and adaptive neural networks. Lin et al. (2014) presented a control protocol based on a complex Laplacian matrix to realize the specified formations using relative positions between agents. Ma et al. (2021) considered the H_∞ cluster formation problem for MASs under external disturbance and random sampling behavior. Furthermore, in fire rescue operations, firefighters need to be divided into several groups to speed up the rescue, which means that a single formation would be inadequate; accordingly, cluster control and scaled control are introduced into MASs corresponding to such circumstances. There have been numerous research results on cluster control for MASs in the literature. Guo et al. (2021) studied cluster consensus with an event-triggered mechanism for MASs with heterogeneous nonlinear second-order dynamics subject to cyber-attacks. Ge et al. (2018) addressed the cluster formation for MASs subject to aperiodic sampling and transmission delays simultaneously. Scaled consensus means that the states of agents can achieve different consensus according to the pre-determined ratios. In this paper a more practical collaborative control of MASs was investigated through combining scaled consensus and formation control.

The communication among agents in cooperative control of MASs is highly dependent on the underlying network topology. Wang H et al. (2019) investigated the fixed-time consensus problem for MASs with nonlinear first-order dynamics in the presence of directed communication topologies. Huang et al. (2020) designed an innovative control protocol to accomplish the consensus of nonlinear MASs exhibiting second-order kinetics. Luo and Ye (2022) investigated the cluster consensus control for linear MASs without regard to the coupling intensities or connection scenarios. Note that the research outcomes derived in Wang H et al. (2019), Huang et al. (2020), and Luo and Ye (2022) were obtained exclusively under fixed network topologies. However, in some cases, such as when there exist cyber-attacks, the original topology structure has to be changed. In response to the switching topologies, agents need to form new formations to complete the tasks. Meng and Jia (2016) solved the consensus problem of MASs with switching topologies, where all agents agree on a value at different time-varying scales. Zhu et al. (2022) considered the formation control for linear MASs with switching directed topologies by proposing two distributed observer-based event-triggered control mechanisms based on absolute or relative outputs. Dong et al. (2017) discussed the time-varying formation tracking problem of MASs with second-order dynamics. Several sufficient and necessary criteria for the feasibility of formation tracking control were given with regard to switching interaction topologies.

In MASs, the states and control information of agents are exchanged through network transmission with high requirements in terms of network bandwidth and hardware equipment (Wang XL et al., 2022). To maximize the utilization of network resources, an event-triggered scheme was introduced. This scheme ensures that the states and control signals of the agents are updated only when specific conditions are ensured, thereby reducing unnecessary communication. Xu and He (2018) considered the cluster consensus control for MASs with a distributed static event-triggered (SET) strategy. To

further achieve the balance between resource saving and system stability, the dynamic event-triggered (DET) mechanism was proposed. It was implemented by introducing an auxiliary dynamic variable (ADV) or a dynamic threshold parameter (DTP). By proposing a distributed DET mechanism involving a DTP, He et al. (2020) studied the consensus problem of linear MASs in leaderless and leader-following topologies under an adaptive control framework. Du et al. (2020) explored the leader-following consensus control in MASs by developing a distributed event-triggered mechanism that incorporates an ADV. Similarly, Ju et al. (2022) studied an ADV-based distributed DET consensus control problem for MASs via fault-estimation-in-the-loop. He and Mo (2022) proposed distributed SET and DET mechanisms for the utilization alleviation of communication resources. The security consensus control for MASs subject to scaling deception attacks was investigated. Note that MASs usually have complex network communication topologies. Thus, it is of significance to explore a better means to balance system stability and network resource saving.

In this study, the scaled formation control for MASs with a modified resilient DET mechanism under fixed and switching topologies is considered. The main contributions are threefold:

1. By introducing a random variable and two different threshold parameters into the traditional DET mechanism, the event-triggering conditions can be adjusted by choosing different threshold parameters according to different statuses of the network, and such an arrangement can enable better use of network resources for the whole system.

2. Different from traditional event-triggered mechanisms where the triggering condition is driven once the combination error term exceeds a certain positive scalar or variable, the absolute value of the combination error term and an ADV are introduced. Thus, the number of event-triggered moments can be effectively reduced and more efficient convergence can be achieved.

3. In the context of MASs with a huge amount of computation, by introducing the sparrow search algorithm (SSA) into the stability criteria for the formation error system in terms of nonlinear matrix inequalities, the control gain can be obtained more reasonably and accurately, thereby reducing the conservatism for control gain design.

2 Preliminaries

2.1 Notations

$\mathbb{N}$ denotes the set of non-negative integers. $\mathbb{R}$ represents the collection of real numbers. $\mathbb{R}^n$ stands for the Euclidean space with n dimensions. $\mathbb{R}^{m\times n}$ means the set of real matrices with $m\times n$ dimensions. col$\{\cdot\}$ represents a column vector. diag$(\cdot)$ denotes a diagonal matrix. $\otimes$ is the Kronecker product. $C>0$ ($C\geq 0$) indicates that matrix C is positive definite (positive semi-definite). I_N expresses the N-dimensional identity matrix. 1_N stands for an N-dimensional column vector where all elements are 1. sgn$[c]$ means the sign of scalar c. $\lambda_{\min}(P)$ denotes the smallest eigenvalue of matrix P. The superscript T represents the transpose of a matrix or a vector. The asterisk $*$ indicates the symmetry in symmetric block matrices. $||\cdot||$ represents the Euclidean norm for a vector or matrix. $|\cdot|$ denotes the absolute value for a scalar. $\mathbb{E}[\cdot]$ is the mathematical expectation operator. $\mathcal{N}_i$ is the set of neighbors of the i^{th} agent.

2.2 Graph theory

$G=\{\mathcal{V},\mathcal{E},\mathcal{A}\}$ refers to a directed graph where $\mathcal{V}=\{v_1,v_2,\cdots,v_N\}$ denotes a set of vertices, $\mathcal{E}\subseteq\mathcal{V}\times\mathcal{V}$ indicates a set of edges and $\mathcal{A}=[a_{ij}]\in\mathbb{R}^{N\times N}$ is a weighed adjacency matrix. $\varepsilon_{ij}=(v_i,v_j)\in\mathcal{E}$ signifies that there exists an edge connecting v_i and v_j, indicating that v_i can receive information from v_j. In other words, v_j is considered a neighbor of v_i. Graph G is said to be strongly connected if there exists a directed path between each pair of vertices (v_i,v_j). For $i\neq j$, if $(v_i,v_j)\in\mathcal{E}$, $a_{ij}\neq 0$; otherwise, $a_{ij}=0$. For any i, $a_{ii}=0$. The Laplacian matrix of G is defined as $L=[l_{ij}]\in\mathbb{R}^{N\times N}$, where l_{ii} is the sum of the weights of all edges incident to vertex v_i, denoted by $\sum_{j\in\mathbb{N}}a_{ij}$, and l_{ij} is equal to the negative weight of the edge connecting vertices v_i and v_j, represented by $-a_{ij}$ for $i\neq j$.

3 Problem statements

3.1 Agent dynamics

Consider a general linear MAS involving N agents. The kinetics of the i^{th} agent is denoted by

$$\dot{x}_i(t)=Ax_i(t)+Bu_i(t),\ \ i=1,2,\cdots,N, \quad (1)$$

where $x_i(t) \in \mathbb{R}^n$ and $u_i(t) \in \mathbb{R}^m$ are the state and the control input of the i^{th} agent, respectively. $A \in \mathbb{R}^{n\times n}$ and $B \in \mathbb{R}^{n\times m}$ are real matrices. This paper aims to propose a scaled formation control framework to ensure that each agent's states in Eq. (1) reach a preset formation according to specified ratios with other agents on its own scale. To do so, the following definitions are presented:

Definition 1 (Roy, 2015) We set a scale vector $\bar{\alpha} = [\alpha_1^{-1}, \alpha_2^{-1}, \cdots, \alpha_N^{-1}]$ where α_i is a non-zero scalar. For arbitrary initial states $x_i(0)$, the scaled consensus for MAS (1) is achieved if

$$\lim_{t\to\infty}\left(\frac{x_i(t)}{\alpha_i} - \frac{x_j(t)}{\alpha_j}\right) = 0. \tag{2}$$

Let $\bar{x}(t) = \frac{1}{N}\sum_{i=1}^{N}\frac{x_i(t)}{\alpha_i}$ represent the scaled average states of the N agents. The required formation is specified by $f(t) = \text{col}\{f_1(t), f_2(t), \cdots, f_N(t)\}$, where $f_i(t)$ is a real vector representing the relative position of the i^{th} agent. Then, scaled formation consensus is further defined.

Definition 2 MAS (1) is defined to asymptotically reach scaled formation consensus if

$$\lim_{t\to\infty}\left(\frac{x_i(t) - f_i(t)}{\alpha_i} - \bar{x}(t)\right) = 0. \tag{3}$$

Remark 1 According to the above definitions, $\lim_{t\to\infty}(\frac{x_i(t)-f_i(t)}{\alpha_i} - \frac{x_j(t)-f_j(t)}{\alpha_j}) = 0$ is established for any $i \neq j$ if $\lim_{t\to\infty}\left(\frac{x_i(t)-f_i(t)}{\alpha_i} - \bar{x}(t)\right) = 0$ holds. As a result, the scaled formation consensus is achieved eventually. Note that the scaled formation is degenerated to a general formation if $\alpha_i = \alpha_j$. The formation is degenerated as one point if $f_i(t) = f_j(t)$. In particular, if $f_i(t) = f_j(t) = 0$, the original scaled formation issue can be reduced to a common scaled consensus problem.

3.2 Modified resilient dynamic event-triggered mechanism

Fig. 1 shows the framework of each agent i. Specifically, the state of the i^{th} agent is sampled by sampler i with a fixed period $h > 0$ with the sampling sequence $\{0h, 1h, 2h, \cdots, \iota h, \cdots\}$ $(\iota \in \mathbb{N})$. The sampled state $x_i(\iota h)$ and its time stamp ι are encapsulated into a sampled-data packet $(x_i(\iota h); \iota)$ and delivered to the event generator of the neighboring nodes. The triggered states of agent i and its neighbors are transmitted to storer i, and finally sent to

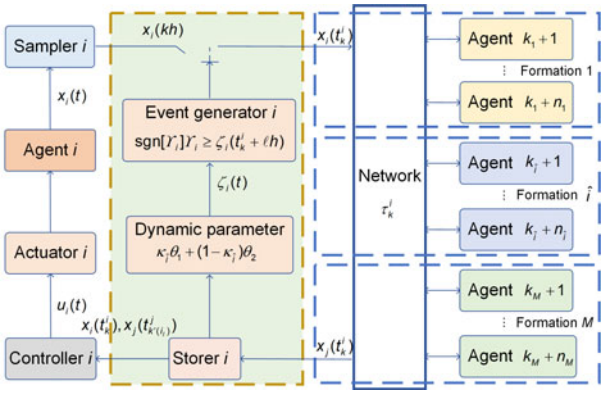

Fig. 1 Scaled formation control framework for the i^{th} agent

controller i to update the control input of the i^{th} agent.

Let us suppose that the triggering sequence for agent i is described as $\{t_0^i, t_1^i, \cdots, t_k^i, \cdots\}$ $(k \in \mathbb{N})$, where t_k^i is the k^{th} event-triggered instant of agent i and $t_0^i = 0$. The next triggering instant t_{k+1}^i is determined by

$$t_{k+1}^i = t_k^i + \inf\{\ell h \mid \text{sgn}[\Upsilon_i]\Upsilon_i \geq \zeta_i(t_k^i + \ell h)\}, \tag{4}$$

where $\ell \in \mathbb{N}$,

$$\Upsilon_i = \delta_i\big(e_i^{\text{T}}(t_k^i + \ell h)\Phi e_i(t_k^i + \ell h) - \sigma_i\chi_i^{\text{T}}(t_k^i)\Omega\chi_i(t_k^i)\big),$$

$\delta_i > 0$, and $\sigma_i > 0$. $\Phi > 0$ and $\Omega > 0$ are the weighting matrices. $e_i(t_k^i + \ell h)$ is denoted as the error variable:

$$e_i(t_k^i + \ell h) = x_i(t_k^i + \ell h) - x_i(t_k^i). \tag{5}$$

$\chi_i(t_k^i)$ is the accumulated error between agents i and j, $i, j = 1, 2, \cdots, N$ and $i \neq j$, and

$$\chi_i(t_k^i) = \sum_{j\in\mathcal{N}_i} a_{ij}\Big(\big(x_i(t_k^i) - f_i(t_k^i)\big) - \alpha_{ij}\big(x_j(t_{k'(i_l)}^j) - f_j(t_{k'(i_l)}^j)\big)\Big),$$

where $\alpha_{ij} = \frac{\alpha_i}{\alpha_j}$. $k'(i_l)$ denotes the latest transmitted data of its neighbors before the current time $t_k^i + \ell h$:

$$k'(i_l) \triangleq \arg\min_l\{t_k^i + \ell h - t_l^j \mid t_k^i + \ell h \geq t_l^j, l \in \mathbb{N}\}. \tag{6}$$

$\zeta_i(t)$ is an auxiliary variable satisfying

$$\dot{\zeta}_i(t) = -\beta_i\zeta_i(t) + \big(\kappa_{\hat{i}}\theta_1 + (1-\kappa_{\hat{i}})\theta_2\big)\text{sgn}[\Upsilon_i]\Upsilon_i, \tag{7}$$

where $\beta_i > 0$ and $\theta_1 > \theta_2 > 0$ are positive constants. $\kappa_{\hat{i}}$ indicates whether the communication channel of

group $\hat{i}$ is busy—when the communication is busy, $\kappa_{\hat{i}}=1$; otherwise, $\kappa_{\hat{i}}=0$. $\hat{i}$ denotes the group in which agent i ($i=1,2,\cdots,N$) is located. When agents i and j are in one group, $\hat{i}=\hat{j}$. It is obvious that agents i and j are in the same group when $\alpha_i=\alpha_j$.

Lemma 1 For prescribed scalars $\delta_i>0$, $\sigma_i\in(0,1)$, and $h>0$, the auxiliary variable $\zeta_i(t+\ell h)$ can be obtained as follows:

$$\begin{aligned}&\zeta_i(t_k^i+\ell h)\\&=\zeta_i(t_k^i)\mathrm{e}^{-\mu\ell h}\int_{t_k^i}^{t_k^i+\ell h}\tilde{\theta}\mathrm{sgn}[\Upsilon_i]\Upsilon_i\mathrm{e}^{-\mu(t_k^i+\ell h-\vartheta)}\mathrm{d}\vartheta,\end{aligned}\tag{8}$$

where $\tilde{\theta}=\kappa_{\hat{i}}\theta_1+(1-\kappa_{\hat{i}})\theta_2$. It can be seen that $\zeta_i(t)$ is monotonically increasing according to $\tilde{\theta}$. Thus, the triggering frequency of the resilient DET mechanism (4) with θ_1 is lower than that with θ_2.

Remark 2 In traditional DET mechanisms, as a measure of the consensus error, Υ_i is sometimes positive and sometimes negative. When Υ_i is positive and the event-triggered condition is researched, the states or control information can be updated; when Υ_i is negative, the event-triggered condition cannot be met. As a result, the convergence performance of the system is not good enough with a considerable total triggering number. In the modified resilient DET mechanism (4) presented in this paper, by introducing the absolute value of Υ_i, the monotonically increasing property can be ensured and the event condition can be triggered when the original Υ_i is negative and not triggered. Therefore, the events can be triggered more reasonably and satisfactory convergence performance can be achieved.

Remark 3 It is known from Lemma 1 that the smaller the parameters $\tilde{\theta}$ are valued, the easier the event is triggered. In the proposed DET mechanism (4), a random variable $\kappa_{\hat{i}}$ is introduced to select two different threshold parameters according to network conditions resiliently. When the network is free, a smaller threshold parameter θ_1 is chosen and the triggering frequency increases; when the network is busy, a larger threshold parameter θ_2 is selected and the triggering frequency decreases. The network resources for the whole system can thus be better used.

3.3 Scaled formation control protocol for a fixed topology

In this subsection, a scaled formation control protocol update strategy with the modified resilient DET mechanism (4) is presented for MAS (1):

$$u_i(t)=K\chi_i(t_k^i),\quad t\in[t_k^i,t_{k+1}^i),\tag{9}$$

where K is the control gain matrix to be designed. Thus, the following closed-loop system can be obtained:

$$\begin{aligned}\dot{x}_i(t)=&Ax_i(t)+BK\sum_{j\in\mathcal{N}_i}a_{ij}\Big(\big(x_i(t_k^i)-f_i(t_k^i)\big)\\&-\alpha_{ij}\big(x_j(t_{k'(t)}^j)-f_j(t_{k'(t)}^j)\big)\Big).\end{aligned}\tag{10}$$

We denote $x(t)=[x_1(t),x_2(t),\cdots,x_N(t)]^{\mathrm{T}}$, $f(t)=[f_1(t),f_2(t),\cdots,f_N(t)]^{\mathrm{T}}$, and set $\varrho_k^ih=t_k^i+\ell h,\ell\in\{0,1,2,\cdots,t_{k+1}^i-t_k^i-1\}$. Let τ_k^i represent the delay of $x_i(t_k^i)$, which is induced by the network and $0<\tau_k^i\le\bar{\tau}_i-h$. We divide up the interval $[t_k^i+\tau_k^i,t_{k+1}^i+\tau_{k+1}^i)$ into a set of subintervals $\Delta_l^i=[\varrho_k^ih+\tau_k^i,\varrho_k^ih+h+\tau_{k+1}^i)$, and denote $\tau_i(t)=t-\varrho_k^ih,t\in\Delta_l^i$, $\tau_i(t)\in(0,\bar{\tau}_i]$; thus, $e(\varrho_k^ih)=e(t-\tau_i(t))=x_i(t_k^i+\ell h)-x_i(t_k^i)$. Therefore, the following closed-loop system can be achieved for $t\in\Delta_l^i$:

$$\begin{aligned}\dot{x}(t)=&(I_N\otimes A)x(t)-\sum_{i=1}^{N}(\alpha L^i\alpha^{-1}\otimes(BK))\big(x(t_k^i)-f(t_k^i)\big)\\=&(I_N\otimes A)x(t)-\sum_{i=1}^{N}(\alpha L^i\alpha^{-1}\otimes(BK))\big(x(t-\tau_i(t))\\&-f(t-\tau_i(t))\big),\end{aligned}\tag{11}$$

where $L^i=\mathrm{diag}(\underbrace{0,\cdots,0}_{i-1},1,\underbrace{0,\cdots,0}_{N-i})L$, and $\alpha=\mathrm{diag}(\alpha_1^{-1},\alpha_2^{-1},\cdots,\alpha_N^{-1})$. We define the error state between agent i and the scaled average value as $z_i(t)=\alpha_i^{-1}x_i(t)-\bar{x}(t)$. Let $z(t)=[z_1(t),z_2(t)\cdots,z_N(t)]^{\mathrm{T}}$. Thus, the matrix form of the error states is obtained as

$$z(t)=\Big(H\alpha^{-1}\otimes I_N\Big)x(t),\tag{12}$$

where $H=I_N-\frac{1}{N}1_N1_N^{\mathrm{T}}$. The derivative of $z(t)$ can be written as

$$\begin{aligned}\dot{z}(t)=&(H\alpha^{-1}\otimes I_N)\dot{x}(t)\\=&(H\alpha^{-1}\otimes A)x(t)-\sum_{i=1}^{N}(HL^i\alpha^{-1}\otimes(BK))\big(x(t-\tau_i(t))\\&-f(t-\tau_i(t))\big).\end{aligned}\tag{13}$$

Therefore, the scaled formation error system can be obtained as

$$\dot{z}(t)=(I_N\otimes A)z(t)-\sum_{i=1}^{N}(HL^iH^{-1}\otimes(BK))z(t-\tau_i(t))+\sum_{i=1}^{N}(HL^i\alpha^{-1}\otimes(BK))f(t-\tau_i(t)). \tag{14}$$

4 Stability analysis under a fixed topology

In this section, the stability of error system (14) will be analyzed.

Theorem 1 Given $\delta_i>0$, $\sigma_i\in(0,1)$, $\beta_i>0$, $\theta_1>\theta_2>0$, $\bar{\tau}_i>0$, $h>0$, scale vector α, and control gain matrix K, system (14) with control protocol (9) and modified resilient DET mechanism (4) is asymptotically stable if there exist matrices $R_\epsilon>0$, $\Phi>0$, $\Omega>0$, and S, such that

$$\Gamma=\begin{bmatrix}\Gamma_{1,1}&\Gamma_{1,2}&\Gamma_{1,3}&\Gamma_{1,4}&0\\ *&\Gamma_{2,2}&\Gamma_{2,3}&\Gamma_{2,4}&0\\ *&*&\Gamma_{3,3}&0&0\\ *&*&*&\Gamma_{4,4}&0\\ *&*&*&*&\Gamma_{5,5}\end{bmatrix}<0, \tag{15}$$

$$\Xi=\begin{bmatrix}U\otimes R_3&U\otimes S\\ *&U\otimes R_3\end{bmatrix}\geq 0, \tag{16}$$

where

$$\begin{aligned}
\Gamma_{1,1}=&U\otimes(2R_1A+R_2-R_3)-\frac{\pi^2}{4}(U\otimes R_4)\\
&+\sum_{i=1}^{N}\bar{\tau}_i^2\big(U\otimes(A^{\mathrm{T}}(R_3+R_4)A)\big),\\
\Gamma_{1,2}=&[\hat{\wp}_1,\hat{\wp}_2,\cdots,\hat{\wp}_N]^{\mathrm{T}},\quad \hat{\wp}_i=-U\otimes S,\\
\Gamma_{1,3}=&[\check{\wp}_1,\check{\wp}_2,\cdots,\check{\wp}_N]^{\mathrm{T}},\quad \check{\wp}_i=-U\otimes(R_2+R_3),\\
\Gamma_{1,4}=&[\acute{\wp}_1,\acute{\wp}_2,\cdots,\acute{\wp}_N]^{\mathrm{T}},\quad \gamma_i=(\tilde{\theta}-\beta_i)\delta_i\mathrm{sgn}[\Upsilon_i],\\
\Gamma_{2,2}=&\mathrm{diag}(\dot{\wp}_1,\dot{\wp}_2,\cdots,\dot{\wp}_N),\\
\Gamma_{2,3}=&\mathrm{diag}(\ddot{\wp}_1,\ddot{\wp}_2,\cdots,\ddot{\wp}_N),\\
\Gamma_{2,4}=&\mathrm{diag}(\tilde{\wp}_1,\tilde{\wp}_2,\cdots,\tilde{\wp}_N),\\
\Gamma_{3,3}=&\mathrm{diag}(\bar{\wp}_1,\bar{\wp}_2,\cdots,\bar{\wp}_N),\\
\Gamma_{4,4}=&\mathrm{diag}(\grave{\wp}_1,\grave{\wp}_2,\cdots,\grave{\wp}_N),\\
\Gamma_{5,5}=&\mathrm{diag}(\gamma_1\Phi,\gamma_2\Phi,\cdots,\gamma_N\Phi),\\
\hat{\wp}_i=&-UHL^iH^{-1}\otimes(2R_1BK)+\frac{\pi^2}{4}(U\otimes R_4)+U\otimes R_3\\
&-U\otimes S-\bar{\tau}_i^2\big(UHL^iH^{-1}\otimes(A^{\mathrm{T}}(R_3+R_4)BK)\big),\\
\acute{\wp}_i=&UHL^i\alpha^{-1}\otimes(2R_1BK)\\
&+\bar{\tau}_i^2\big(UHL^i\alpha^{-1}\otimes(A^{\mathrm{T}}(R_3+R_4)BK)\big),\\
\dot{\wp}_i=&\bar{\tau}_i^2\big(H^{-\mathrm{T}}(L^i)^{\mathrm{T}}H^{\mathrm{T}}UHL^iH^{-1}\otimes(K^{\mathrm{T}}B^{\mathrm{T}}(R_3+R_4)\cdot BK)\big)-2U\otimes R_3+U\otimes S+U\otimes S^{\mathrm{T}}-\frac{\pi^2}{4}(U\otimes R_4)-\gamma_i\sigma_i(H^{-\mathrm{T}}(L^i)^{\mathrm{T}}H^{\mathrm{T}}\Omega HL^iH^{-1}\otimes I_N),\\
\tilde{\wp}_i=&-\bar{\tau}_i^2\big(H^{-\mathrm{T}}(L^i)^{\mathrm{T}}H^{\mathrm{T}}UHL^i\alpha^{-1}\otimes(K^{\mathrm{T}}B^{\mathrm{T}}\big(R_3+R_4\big)\cdot BK)\big)+\gamma_i\sigma_i(H^{-\mathrm{T}}(L^i)^{\mathrm{T}}H^{\mathrm{T}}\Omega HL^i\alpha^{-1}\otimes I_N),\\
\ddot{\wp}_i=&U\otimes(R_3-S),\\
\grave{\wp}_i=&\bar{\tau}_i^2\big(\alpha^{-\mathrm{T}}(L^i)^{\mathrm{T}}H^{\mathrm{T}}UHL^i\alpha^{-1}\otimes(K^{\mathrm{T}}B^{\mathrm{T}}(R_3+R_4)\cdot BK)\big)-\gamma_i\sigma_i(\alpha^{-\mathrm{T}}(L^i)^{\mathrm{T}}H^{\mathrm{T}}\Omega HL^i\alpha^{-1}\otimes I_N).
\end{aligned}$$

Proof See Appendix A.

5 Scaled formation control protocol for a switching topology

When the MASs are assigned to form several formations to complete complicated tasks, the topology connection may be destroyed due to the varying environment or unexpected incidents such as denial of service (DoS) attacks. The number of groups, the number of agents in each group, and the connection topology need to be re-allocated to cope with the actual situations. In this section, the switching topology caused by DoS attacks obeying the Markov chain (Ye N et al., 2004) is considered.

We set $G(\omega(t))=\{G_1,G_2,\cdots,G_r\}\,(r\in\mathbb{N})$ as the set of all possible topologies, where $\omega(t)$ is a continuous-time Markov process with its values taken in a finite set $\mathcal{R}=\{1,2,\cdots,r\}$. $\Pi=[\xi_{bd}]$ is defined as the transition rate matrix with $b,d\in\mathcal{R}$. The transition probabilities can be given by

$$\mathrm{Prob}\{\omega(t+\triangle t)=d|\omega(t)=b\}=\begin{cases}\xi_{bd}\triangle t+o(\triangle t), & b\neq d,\\ 1+\xi_{bd}\triangle t+o(\triangle t), & b=d,\end{cases} \tag{17}$$

where $\Delta t>0$ and $\lim_{\Delta t\to 0}o(\triangle t)$. $\xi_{bd}>0$ is the transition rate at which the state b at time t switches to state d at time $t+\triangle t$, and $\xi_{dd}=-\sum_{b=1,b\neq d}\xi_{bd}$ when $b=d$. The corresponding Laplacian matrix is denoted as $L(\omega(t))=\{L_1,L_2,\cdots,L_r\}$. Then, under the Markov switching topologies and the modified resilient DET mechanism (4), the control protocol is presented as follows:

$$u_i(t)=K(\omega(t_k^i))\sum_{j\in\mathcal{N}_i}a_{ij}(\omega(t_k^i))\Big(\big(x_i(t_k^i)-f_i(t_k^i)\big)$$

$$-\alpha_{ij}(\omega(t_k^i))\big(x_j(t^j_{k'(i_l)})-f_j(t^j_{k'(i_l)})\big)\Big), \quad (18)$$

where $t\in[t_k^i,t_{k+1}^i)$, and $K(\omega(t_k^i))$ is the control gain matrix to be designed.

The error system can be obtained by applying the designed control protocol (18):

$$\dot{z}(t)=(I_N\otimes A)z(t)-\sum_{i=1}^{N}(HL_b^iH^{-1}\otimes BK_b)z(t-\tau_i(t))+\sum_{i=1}^{N}(HL_b^i\alpha_b^{-1}\otimes BK_b)f(t-\tau_i(t)), \quad (19)$$

where $K_b=K(\omega(t_k^i))$, $L_b=L(\omega(t_k^i))$, $\alpha_b=\alpha(\omega(t_k^i))$, and $L_b^i=\mathrm{diag}(\underbrace{0,\cdots,0}_{i-1},1,\underbrace{0,\cdots,0}_{N-i})L_b$. The initial condition of the state $z(t)$ is supplied by $z(\theta)=\psi(\theta),\theta\in[-\bar{\tau},0]$ with $\psi(0)=z(0)$ and $\psi\in\Theta$, where Θ represents the Banach space of absolutely continuous functions $[-\bar{\tau},0]\to\mathbb{R}^{nN}$ with square-integrable derivatives and the norm $\|\psi\|_\Theta=\max_{\theta\in[-\bar{\tau},0]}\|\psi(\theta)\|+(\int_{-\bar{\tau}}^{0}\|\dot{\psi}(s)\|^2\mathrm{d}s)^{1/2}$.

Definition 3 (Yu JJ et al., 2009) Under any initial conditions, system (19) is exponentially stable in the sense of mean square, if there exist positive scalars ε and ν such that

$$\mathbb{E}\{\|z(t)\|^2\}\le\varepsilon\mathrm{e}^{-\nu t}\sup_{-\bar{\tau}\le\theta\le0}\mathbb{E}\{\|\psi(\theta)\|^2\}. \quad (20)$$

6 Stability analysis under a switching topology

In this section, the stability of scaled formation error system (19) is analyzed.

Theorem 2 Given $\delta_i>0$, $\sigma_i\in(0,1)$, $\beta_i>0$, $\theta_1>\theta_2>0$, $\bar{\tau}_i>0$, $h>0$, Π, scale vector α_b, and control gain matrix K_b, system (19) with the proposed control protocol (9) and modified resilient DET mechanism (4) under switching topologies is exponentially stable in the mean square sense if there exist matrices $R_1^b>0$, $R_\epsilon>0$, $\Phi>0$, $\Omega>0$, and S such that inequality (16) is satisfied and

$$\Psi=\begin{bmatrix}\Psi_{1,1}&\Psi_{1,2}&\Psi_{1,3}&\Psi_{1,4}&0\\ *&\Psi_{2,2}&\Psi_{2,3}&\Psi_{2,4}&0\\ *&*&\Psi_{3,3}&0&0\\ *&*&*&\Psi_{4,4}&0\\ *&*&*&*&\Psi_{5,5}\end{bmatrix}<0, \quad (21)$$

where

$$\Psi_{1,1}=U\otimes\left(2\sum_{d=1}^{r}\xi_{bd}R_1^bA+R_2+R_3\right)-\frac{\pi^2}{4}(U\otimes R_4)+\sum_{i=1}^{N}\bar{\tau}_i^2\big(U\otimes(A^{\mathrm{T}}(R_3+R_4)A)\big),$$

$$\Psi_{1,2}=[\hat{\Im}_1,\hat{\Im}_2,\cdots,\hat{\Im}_N]^{\mathrm{T}},$$

$$\Psi_{2,2}=\mathrm{diag}(\grave{\Im}_1,\grave{\Im}_2,\cdots,\grave{\Im}_N),$$

$$\Psi_{1,3}=[\check{\Im}_1,\check{\Im}_2,\cdots,\check{\Im}_N]^{\mathrm{T}},\ \check{\Im}_i=U\otimes\hat{S},$$

$$\Psi_{2,4}=\mathrm{diag}(\tilde{\Im}_1,\tilde{\Im}_2,\cdots,\tilde{\Im}_N),$$

$$\Psi_{1,4}=[\acute{\Im}_1,\acute{\Im}_2,\cdots,\acute{\Im}_N]^{\mathrm{T}},$$

$$\Psi_{3,3}=\mathrm{diag}(\bar{\Im}_1,\bar{\Im}_2,\cdots,\bar{\Im}_N),\ \bar{\Im}_i=U\otimes(R_3-R_2),$$

$$\Psi_{2,3}=\mathrm{diag}(\ddot{\Im}_1,\ddot{\Im}_2,\cdots,\ddot{\Im}_N),\ \ddot{\Im}_i=U\otimes(R_3-\hat{S}),$$

$$\Psi_{4,4}=\mathrm{diag}(\dot{\Im}_1,\dot{\Im}_2,\cdots,\dot{\Im}_N),$$

$$\Psi_{5,5}=\mathrm{diag}(\gamma_1\Phi,\gamma_2\Phi,\cdots,\gamma_N\Phi),$$

$$\hat{\Im}_i=-UHL_b^iH^{-1}\otimes\left(2\sum_{d=1}^{r}\xi_{bd}R_1^bBK_b\right)+\frac{\pi^2}{4}(U\otimes R_4)-\bar{\tau}_i^2\big(UHL_b^iH^{-1}\otimes(A^{\mathrm{T}}(R_3+R_4)BK_b)\big)+U\otimes(R_3-\hat{S}),$$

$$\acute{\Im}_i=2UHL_b^i\alpha_b^{-1}\otimes\left(\sum_{d=1}^{r}\xi_{bd}R_1^bBK_b\right)+\bar{\tau}_i^2\big(UHL_b^i\alpha_b^{-1}\otimes\big(A^{\mathrm{T}}(R_3+R_4)BK_b\big)\big),$$

$$\grave{\Im}_i=\bar{\tau}_i^2\big(H^{-\mathrm{T}}(L_b^i)^{\mathrm{T}}H^{\mathrm{T}}UHL_b^iH^{-1}\otimes(K_b^{\mathrm{T}}B^{\mathrm{T}}(R_3+R_4)\cdot BK_b)\big)-\gamma_i\sigma_i(H^{-\mathrm{T}}(L_b^i)^{\mathrm{T}}H^{\mathrm{T}}\Omega HL_b^iH^{-1}\otimes I_N),-\frac{\pi^2}{4}(U\otimes R_4)+U\otimes(\hat{S}+\hat{S}^{\mathrm{T}}-2R_3),$$

$$\tilde{\Im}_i=-\bar{\tau}_i^2\big(H^{-\mathrm{T}}(L_b^i)^{\mathrm{T}}H^{\mathrm{T}}UHL_b^i\alpha_b^{-1}\otimes(K_b^{\mathrm{T}}B^{\mathrm{T}}(R_3+R_4)\cdot BK_b)\big)+\gamma_i\sigma_i(H^{-\mathrm{T}}(L_b^i)^{\mathrm{T}}H^{\mathrm{T}}\Omega HL_b^i\alpha_b^{-1}\otimes I_N),$$

$$\dot{\Im}_i=\bar{\tau}_i^2\big(\alpha_b^{-\mathrm{T}}(L_b^i)^{\mathrm{T}}H^{\mathrm{T}}UHL_b^i\alpha_b^{-1}\otimes(K_b^{\mathrm{T}}B^{\mathrm{T}}(R_3+R_4)\cdot BK_b)\big)-\gamma_i\sigma_i(\alpha_b^{-\mathrm{T}}(L_b^i)^{\mathrm{T}}H^{\mathrm{T}}\Omega HL_b^i\alpha_b^{-1}\otimes I_N),$$

$$\gamma_i=(\tilde{\theta}-\beta_i)\delta_i\mathrm{sgn}[\Upsilon_i].$$

Proof See Appendix B.

7 SSA-based control and triggering parameter co-design

It can be seen that matrix inequality (15) in Theorem 1 is nonlinear because of the coupling of variable matrices R_1, R_3, R_4 and control matrix K. Similarly, the coupling of R_1^b and control matrix K_b results in the nonlinearity in matrix inequality (21) in Theorem 2. One can transform nonlinear inequalities into linear inequalities by applying traditional linearization techniques such as iterative linear matrix inequality (ILMI), cone complementarity linearization (CCL), and the state-space transformation

approach, and then calculate the control gain matrix via the MATLAB LMI toolbox. However, on one hand, traditional linearization methods may introduce a certain amount of conservatism, and on the other hand, there may be limited scalability, especially for high dimensions of matrix inequalities for MASs, which usually possess numerous nodes and complex topological connections. Therefore, it is important to develop an effective algorithm to compute the triggering parameters, weighting matrix, and control gain jointly in the context of MASs.

SSA is a nature-inspired optimization algorithm that draws inspiration from the foraging and predator avoidance behaviors exhibited by sparrows (Xue and Shen, 2020). Specifically, the sparrows are classified into three categories: discoverer, joiner, and scout. The discoverers, commonly possessing a high fitness value, are in charge of offering fields and directions of foraging for joiners. The joiners monitor and follow the discoverers constantly for earning better food. When the scouts spot predators, they emit warning signals, as a result of which the whole community of sparrows would instantly show predation behavior. The fitness function is designed as the distance between each sparrow and food. The next movement direction of the sparrow group can be determined using the optimal fitness value. This innovative algorithm showcases remarkable optimization capabilities and exhibits high convergence speed.

In this section, SSA is applied to compute the control gain matrix and triggering parameters in the framework of MASs by dealing with the nonlinear inequalities directly. The control gains and triggering parameters are defined as the sparrow positions, and the scaled formation error state is viewed as the fitness value. The pseudo code of the SSA-based control and triggering parameter co-design is shown in Algorithm 1. The following descriptions provide a comprehensive breakdown of the detailed design process: Step 1: initialize parameters. The maximum number of iterations is set as iter and the sparrow cluster size as num. The initial position of the sparrow (i.e., the control gain K) is randomly selected while the conditions in Theorem 1 or 2 are ensured.

Step 2: design the fitness function. The fitness function is designed as the scaled formation error state for each sparrow. The best position is obtained when the fitness function reaches its minimum value, and the worst position is obtained when the maximum fitness value is reached.

Step 3: update sparrow positions. t is set as the current iteration. $k_{i,j}^{\mathrm{d}}(t)$, $k_{i,j}^{\mathrm{e}}(t)$, and $k_{i,j}^{\mathrm{s}}(t)$ denote the positions in the j^{th} dimension in the t^{th} iteration of the i^{th} sparrow, which may be categorized variously into discoverer, joiner, and scout, respectively. The updating rules are as follows:

$$k_{i,j}^{\mathrm{d}}(t+1)=\begin{cases} k_{i,j}^{\mathrm{d}}(t)\exp(-\frac{i}{u\cdot\mathrm{iter}}), & \rho<\mathrm{ST},\\ k_{i,j}^{\mathrm{d}}(t)+\mu\upsilon, & \rho\geq\mathrm{ST}, \end{cases} \tag{22}$$

$$k_{i,j}^{\mathrm{e}}(t+1) =\begin{cases} \mu\exp\left(\frac{k_{\mathrm{worst}}(t)-k_{i,j}^{\mathrm{e}}(t)}{i^2}\right), & i>\frac{N}{2},\\ k_{\mathrm{best}}(t+1)+|k_{i,j}^{\mathrm{e}}(t)-k_{\mathrm{best}}(t+1)|J^{+}\upsilon, & i\leq\frac{N}{2}, \end{cases} \tag{23}$$

$$k_{i,j}^{\mathrm{s}}(t+1) =\begin{cases} k_{\mathrm{best}}(t)+\varpi|k_{i,j}^{\mathrm{s}}(t)-k_{\mathrm{best}}(t)|, & f_i>f_{\mathrm{b}},\\ k_{i,j}^{\mathrm{s}}(t)+c\frac{|k_{i,j}^{\mathrm{s}}(t)-k_{\mathrm{worst}}(t)|}{f_i(t)-f_{\mathrm{w}}(t)+\varsigma}, & f_i\leq f_{\mathrm{b}}. \end{cases} \tag{24}$$

Herein $u\in[0,1]$ and $\rho\in[0,1]$ are the stochastic variables for warning; $\mathrm{ST}\in[0.5,1]$ is the safety value; μ is the stochastic variable obeying the normal distribution; $\upsilon\in\mathbb{R}^{1\times\dim}$ is the matrix where each element is 1; $J^{+}=J^{\mathrm{T}}(JJ^{-1})^{-1}$, where J is a column vector with the same dimension as each sparrow, and the internal elements of J are composed of 1 and -1; ϖ is a random parameter obeying the normal distribution, and refers to the step of position updating; $c\in[-1,1]$ is a stochastic variable; f_i denotes the fitness function of the current sparrow individual; f_{b} and f_{w} are the best and worst fitness values, respectively; $k_{\mathrm{best}}(t)$ and $k_{\mathrm{worst}}(t)$ are the best and worst positions, respectively; ς is a small constant.

8 Numerical examples

In this section, a simulation platform of a system with multiple unmanned aerial vehicles (UAVs) is set up to confirm the validity of the presented scaled formation control protocols (9) and (18) and the proposed modified DET mechanism (4).

8.1 Multi-UAV system

The kinematic equation of quarotor UAV i presented in Fig. 2 (the related parameters are described

Algorithm 1 SSA-based control design algorithm

Input: num, iter, dim, u, ρ, ST, μ, υ, J, ϖ, c, ε, δ_i, σ_i, β_i, θ_{1i}, θ_{2i}, h, $\bar{\tau}_i^p$, $f_i(t)$, $f_i'(t)$, $\alpha(t)$, $\alpha'(t)$, $x_i(0)$, k-range
Output: k_{best}, R_1^p, R_ϵ, Φ, and Ω
Set num, iter, dim, u, ρ, ST, μ, υ, J, ϖ, c, ε, δ_i, σ_i, β_i, θ_{1i}, θ_{2i}, h, $\bar{\tau}_i^p$, $f_i(t)$, $f_i'(t)$, $\alpha(t)$, $\alpha'(t)$, $x_i(0)$, k-range
Initialize k_i^0 and calculate the individual fitness
Update k_{best}^0 and k_{worst}^0
$t=1$
loop
  Judge whether the matrix inequalities in Theorem 1 or 2 are satisfied
  for $i=1:\text{num}\times 0.7$ **do**
    for $j=1:\text{dim}$ **do**
      Update the positions of discoverers
    end for
  end for
  for $i=1:\text{num}\times 0.1$ **do**
    for $j=1:\text{dim}$ **do**
      Update the positions of joiners
    end for
  end for
  for $i=1:\text{num}\times 0.2$ **do**
    for $j=1:\text{dim}$ **do**
      Update the positions of scouts
    end for
  end for
  Calculate the fitness value
  Update $f_{\text{b}}(t)$ and $f_{\text{w}}(t)$
  Update $k_{\text{best}}(t)$ and $k_{\text{worst}}(t)$
  $t=t+1$
  Record $k_{\text{best}}(t)$
end loop

in Table 1) is represented by

$$m_i\begin{bmatrix}\ddot{X}_i\\ \ddot{Y}_i\\ \ddot{Z}_i\end{bmatrix}=\begin{bmatrix}0\\0\\m_ig\end{bmatrix}+R\begin{bmatrix}0\\0\\-F_i\end{bmatrix}, \tag{25}$$

where

$$R=\begin{bmatrix}\theta_{\text{c}}\psi_{\text{c}} & \psi_{\text{c}}\phi_{\text{s}}\theta_{\text{s}}-\phi_{\text{c}}\psi_{\text{s}} & \phi_{\text{s}}\psi_{\text{s}}+\phi_{\text{c}}\psi_{\text{c}}\theta_{\text{s}}\\ \theta_{\text{c}}\psi_{\text{s}} & \psi_{\text{c}}\phi_{\text{c}}+\phi_{\text{s}}\theta_{\text{s}}\psi_{\text{s}} & \phi_{\text{c}}\theta_{\text{s}}\psi_{\text{s}}-\phi_{\text{c}}\psi_{\text{s}}\\ -\theta_{\text{s}} & \theta_{\text{c}}\phi_{\text{s}} & \phi_{\text{c}}\theta_{\text{c}}\end{bmatrix},$$

$\phi_{\text{s}}=\sin\phi$, $\phi_{\text{c}}=\cos\phi$, $\theta_{\text{s}}=\sin\theta$, $\theta_{\text{c}}=\cos\theta$, $\psi_{\text{s}}=\sin\psi$, and $\psi_{\text{c}}=\cos\psi$.

Thus, the decomposition of Eq. (25) in the X and Y directions can be obtained as

$$\begin{cases}m_i\ddot{X}_i=-F_i(\phi_{\text{s}}\psi_{\text{s}}+\phi_{\text{c}}\psi_{\text{c}}\theta_{\text{s}}),\\ m_i\ddot{Y}_i=-F_i(\phi_{\text{c}}\psi_{\text{s}}-\phi_{\text{c}}\psi_{\text{c}}\theta_{\text{s}}).\end{cases} \tag{26}$$

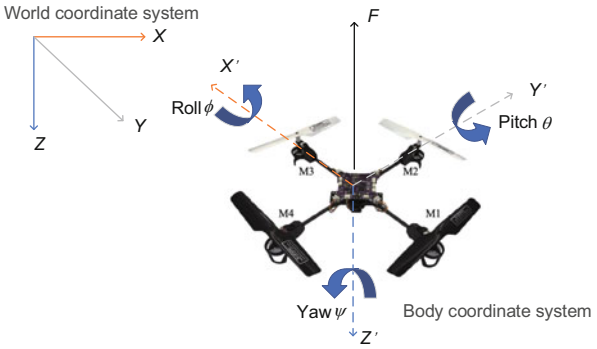

Fig. 2 Quadrotor UAV schematic

Table 1 Parameters of UAV i

Parameter	Meaning
m_i	Weight of UAV i
F_i	Synthetic external force acting on UAV i
X_i	Position decomposition in the X direction in the realistic spatial coordinate system for UAV i
Y_i	Position decomposition in the Y direction in the realistic spatial coordinate system for UAV i
Z_i	Position decomposition in the Z direction in the realistic spatial coordinate system for UAV i
ϕ	Roll angle
θ	Pitch angle
ψ	Yaw angle
g	Gravitational acceleration
R	Transformation matrix from the body coordinate system to the realistic spatial coordinate system

Linearization can be performed according to the following principles (Ren and Atkins, 2005): (1) Given that θ and ϕ are very small angles, it may be established that $\theta_{\text{s}}\approx 0, \phi_{\text{s}}\approx 0, \theta_{\text{c}}\approx 1$, and $\phi_{\text{c}}\approx 1$; (2) If the hovering of the UAV is nearly steady, $F_i=m_ig$; (3) We may assume that the desired yaw angle $\psi=0$. As a result, Eq. (25) can be rewritten as

$$\ddot{X}_i=u_{xi},\quad \ddot{Y}_i=u_{yi},$$

where $u_{xi}=-g\theta$ and $u_{yi}=g\phi$ are the decomposition of control input in the X and Y directions (Mahony et al., 2012; Wang JH et al., 2020), respectively.

Thus, the description in Eq. (25) can be

linearized as

$$\begin{cases} \dot{p}_{\star i} = v_{\star i}(t), \\ \dot{v}_{\star i} = u_{\star i}(t), \end{cases} \tag{27}$$

where $\star$ represents X or Y. $p_{\star i}(t)$, $v_{\star i}(t)$, and $u_{\star i}(t)$ are the displacement, velocity, and control input components for the X (or Y) axis, respectively.

We denote $x_i(t) = \mathrm{col}\{p_{xi}(t), v_{xi}(t), p_{yi}(t), v_{yi}(t)\}$ and $u_i(t) = \mathrm{col}\{u_{xi}(t), u_{yi}(t)\}$. Eq. (27) can be rewritten as

$$\dot{x}_i(t) = Ax_i(t) + Bu_i(t), \tag{28}$$

where $A = \begin{bmatrix} 0 & 1 & 0 & 0 \\ 0 & 0 & 0 & 0 \\ 0 & 0 & 0 & 1 \\ 0 & 0 & 0 & 0 \end{bmatrix}$ and $B = \begin{bmatrix} 0 & 0 \\ 1 & 0 \\ 0 & 0 \\ 0 & 1 \end{bmatrix}$.

8.2 Scaled formation control under a fixed topology

The scaled formation flying is accomplished if the position states achieve a pre-set formation with a certain scale and the velocity states reach the same value. The underlying topology is illustrated in Fig. 3, where an arrangement is presented by which the 12 UAVs are required to take up a threesome formation through the determination of an appropriate scale vector.

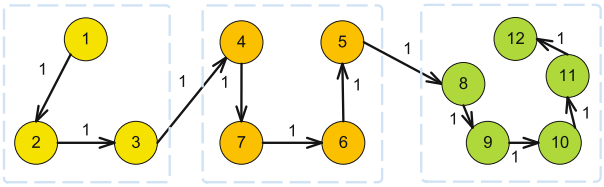

Fig. 3 Topology G_1

Let $h = 0.01$ and $\bar{\tau}_1 = 0.5$. The formation information and initial states of UAVs 1–12 are given in Table 2. We set $\zeta_{1i}(0) = \zeta_{2i}(0) = 1$. The triggering parameters δ_i, σ_i, β_i, θ_{1i}, and θ_{2i} are valued in Table 3. The scale vector under the fixed topology is set as $\alpha_1 = \left[1, 1, 1, \frac{1}{2.5}, \frac{1}{2.5}, \frac{1}{2.5}, \frac{1}{2.5}, \frac{1}{4}, \frac{1}{4}, \frac{1}{4}, \frac{1}{4}, \frac{1}{4}\right]$. By dealing with criteria (15) and (16) in Theorem 1 and the SSA-based co-design algorithm, the triggering weighting matrices $\Phi = \begin{bmatrix} 1.5 & 0.3 & 0.3 & 0.3 \\ 0.3 & 1.5 & 0.3 & 0.3 \\ 0.3 & 0.3 & 1.5 & 0.3 \\ 0.3 & 0.3 & 0.3 & 1.5 \end{bmatrix}$ and $\Omega = \begin{bmatrix} 2 & 0.2 & 0.2 & 0.2 \\ 0.2 & 2 & 0.2 & 0.2 \\ 0.2 & 0.2 & 2 & 0.2 \\ 0.2 & 0.2 & 0.2 & 2 \end{bmatrix}$, and the control gain matrix $K_1 = \begin{bmatrix} 13.6785 & 14.3422 & 0 & 0 \\ 0 & 0 & 13.6785 & 14.3422 \end{bmatrix}$ can be calculated. Fig. 4 depicts the position trajectories of UAVs 1–12. It is easy to see that the positions of UAVs 1–3 achieve a triangular formation, those of UAVs 4–7 a square, and those of UAVs 8–12 a pentagon. Fig. 5 presents the X- and Y-axis components of the velocity state responses of the 12 UAVs. Fig. 6 plots the sequences of event-triggered moments of UAVs 1–12 based on the modified DET mechanism (4).

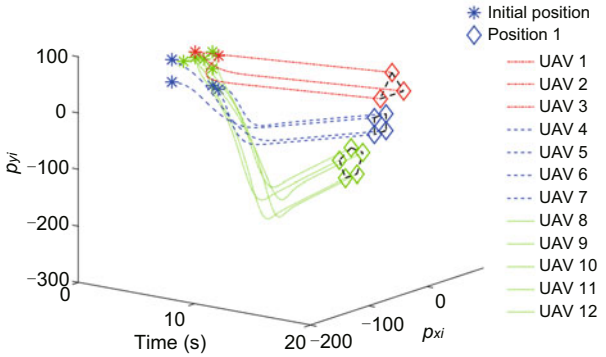

Fig. 4 Position states of UAVs 1–12 under G_1 ($i = 1, 2, \cdots, 12$)

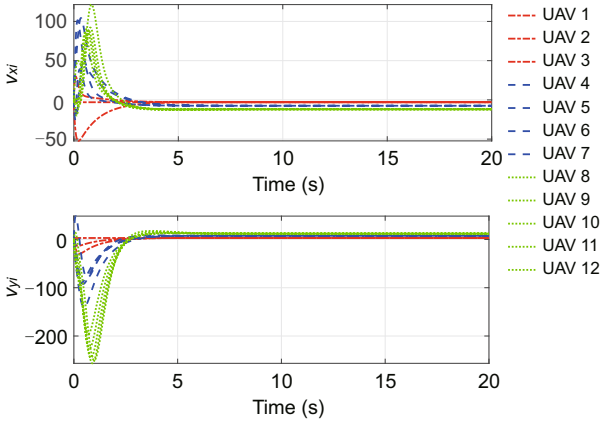

Fig. 5 Velocity states of UAVs 1–12 under G_1 ($i = 1, 2, \cdots, 12$)

Table 2 Formation information and the initial states of UAV$_i$

UAV No.	Fixed-topology formation $f_i(t)$	Switching-topology formation $f_i'(t)$	Initial state $x_i(0)$
1	[0; 0; 140; 0]	[10; 0; 30; 0]	[0; −3; 40; 3]
2	[−20; 0; 100; 0]	[31; 0; 21; 0]	[40; −4; 20; −2]
3	[20; 0; 100; 0]	[250; 0; −80; 0]	[0; −1; 40; −1]
4	[60; 0; 130; 0]	[40; 0; 0; 0]	[−40; 3; 0; 4]
5	[80; 0; 130; 0]	[31; 0; −21; 0]	[40; 2; −40; 4]
6	[80; 0; 100; 0]	[10; 0; −30; 0]	[−40; 4; 40; −2]
7	[60; 0; 100; 0]	[230; 0; −100; 0]	[30; −1; −30; 1]
8	[110; 0; 150; 0]	[−11; 0; −21; 0]	[30; −4; 0; −2]
9	[90; 0; 135; 0]	[−20; 0; 0; 0]	[0; 2; 30; −3]
10	[100; 0; 100; 0]	[−11; 0; 21; 0]	[15; −3; 22; −2]
11	[120; 0; 100; 0]	[250; 0; −120; 0]	[30; −1; 30; −1]
12	[130; 0; 135; 0]	[270; 0; −100; 0]	[−20; −1; 30; −1]

Table 3 Parameter values

UAV No.	δ_i	σ_i	β_i	θ_{1i}	θ_{2i}	UAV No.	δ_i	σ_i	β_i	θ_{1i}	θ_{2i}
1	0.002	0.007	0.02	0.1	0.001	7	0.001	0.007	0.04	0.1	0.001
2	0.003	0.008	0.01	0.1	0.001	8	0.003	0.009	0.04	0.1	0.001
3	0.004	0.006	0.02	0.1	0.001	9	0.004	0.006	0.04	0.1	0.001
4	0.004	0.009	0.03	0.1	0.001	10	0.005	0.007	0.05	0.1	0.001
5	0.003	0.007	0.02	0.1	0.001	11	0.001	0.008	0.03	0.1	0.001
6	0.002	0.008	0.03	0.1	0.001	12	0.003	0.009	0.02	0.1	0.001

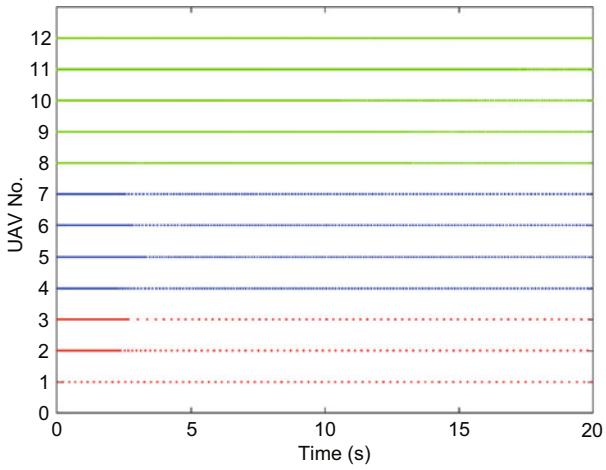

Fig. 6 Triggering instant sequences of UAVs 1–12 under G_1

8.3 Scaled formation control under a switching topology

The communication topology is considered switching between G_1 and G_2 (Fig. 7) obeying a Markov switching chain with the transformation matrix $\Pi = \begin{bmatrix}0.7 & 0.3\\ 0.4 & 0.6\end{bmatrix}$. Correspondingly, the scale vector changes between $\alpha_2 = \left[1,1,1,\frac{1}{2},\frac{1}{2},\frac{1}{2},\frac{1}{2},\frac{1}{3},\frac{1}{3},\frac{1}{3},\frac{1}{3},\frac{1}{3}\right]$ and $\alpha_2' = \left[1,1,\frac{1}{2},1,1,1,\frac{1}{2},1,1,1,\frac{1}{2},\frac{1}{2}\right]$. The formation information and the initial states of UAVs 1–12 are listed in Table 2. We set $\bar{\tau}_2 = 2$. The other parameters are the same as those under a fixed topology in Section 8.2. In terms of criterion (16) in Theorem 1 and criterion (21) in Theorem 2, and by applying the SSA-based co-design algorithm (Algorithm 1), the triggering weighting matrices $\Phi = \begin{bmatrix}1.5 & 0.3 & 0.3 & 0.3\\ 0.3 & 1.5 & 0.3 & 0.3\\ 0.3 & 0.3 & 1.5 & 0.3\\ 0.3 & 0.3 & 0.3 & 1.5\end{bmatrix}$ and $\Omega = \begin{bmatrix}2 & 0.2 & 0.2 & 0.2\\ 0.2 & 2 & 0.2 & 0.2\\ 0.2 & 0.2 & 2 & 0.2\\ 0.2 & 0.2 & 0.2 & 2\end{bmatrix}$, and the control gain matrices $K_2 = \begin{bmatrix}12.6785 & 13.3422 & 0 & 0\\ 0 & 0 & 12.6785 & 13.3422\end{bmatrix}$ and $K_2' = \begin{bmatrix}14.8875 & 15.4875 & 0 & 0\\ 0 & 0 & 14.8875 & 15.4875\end{bmatrix}$, are obtained.

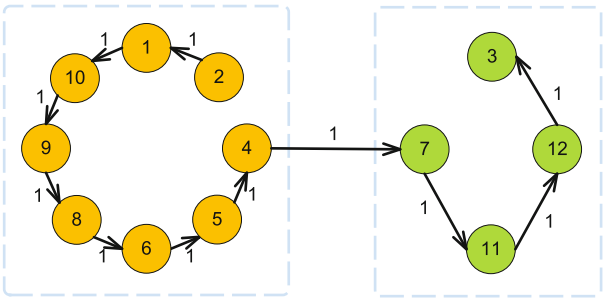

Fig. 7 Topology G_2

Fig. 8 depicts the position trajectories of UAVs 1–12 during the entire running time of 0–20 s. Figs. 9 and 10 depict the position trajectories of the UAVs before and after topology switching, respectively. It can be seen that during 0–10 s, the positions of UAVs 1–3 achieve a triangular formation, those of UAVs 4–7 a square, and those of UAVs 8–12 a pentagon. During 10–20 s, the positions of UAVs 1, 2, 4–6, and 8–10 transform into the formation of a circle, and those of UAVs 3, 7, 11, and 12 into that of a rhombus. Fig. 11 presents the X- and Y-axis components of the velocity state responses of the 12 UAVs. Fig. 12 gives the triggering sequences of UAVs 1–12 based on the modified DET mechanism (4).

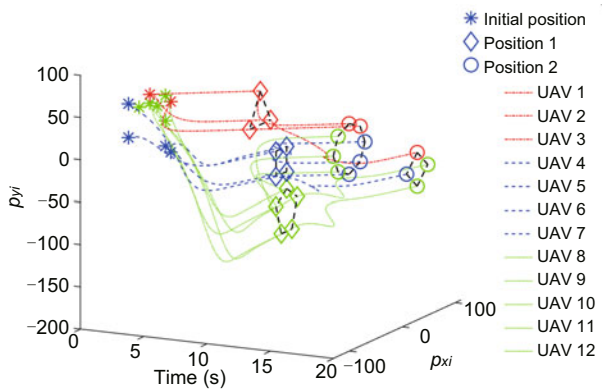

Fig. 8 Position states of UAVs 1–12 under G_1 and G_2 ($i = 1, 2, \cdots, 12$)

8.4 Comparison and discussions

For comparison, four different event-triggered schemes are employed. The total triggering number and errors are obtained and listed in Tables 4 and 5 for fixed and switching topologies, respectively. Table 4 shows that, pursuant to the use of a modified resilient DET mechanism (4) with an absolute value, the required formation control can be reached under a fixed topology with a smaller error, as well as a greater number of instances characterized by a small triggering number. Table 5 shows that the proposed modified resilient DET mechanism (4) exhibits better performance in realizing the expected formation control under a switching topology with a reduced error, while maintaining the same level in terms of the number of instances of triggering.

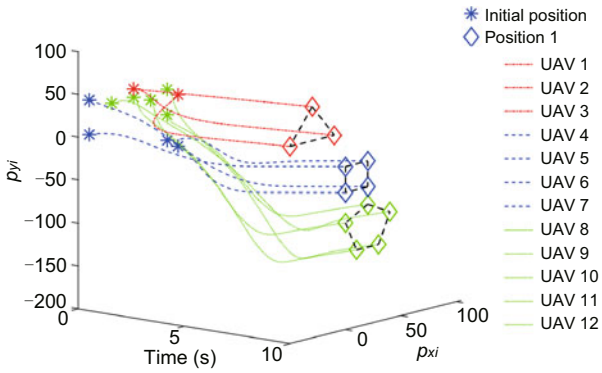

Fig. 9 Position states of UAVs 1–12 under G_1 in [0, 10] s ($i = 1, 2, \cdots, 12$)

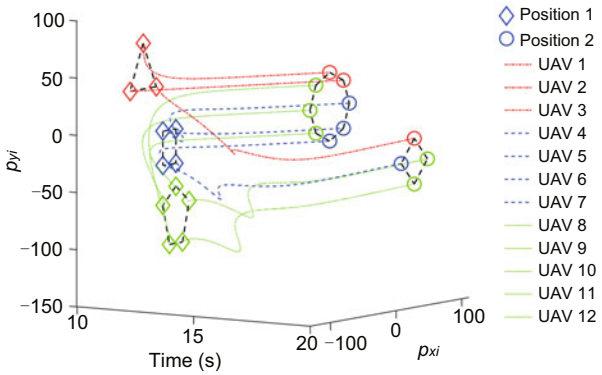

Fig. 10 Position states of UAVs 1–12 under G_2 in [10, 20] s ($i = 1, 2, \cdots, 12$)

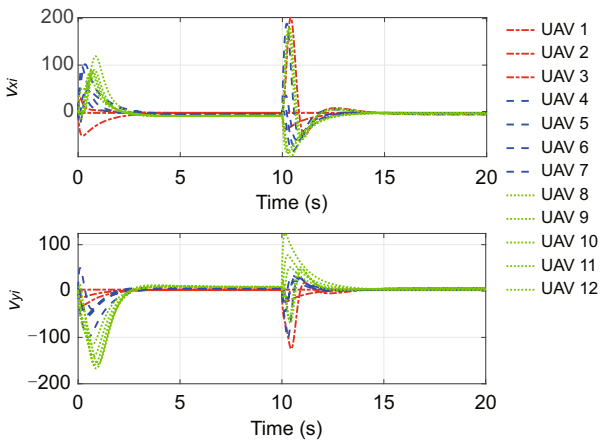

Fig. 11 Velocity states of UAVs 1–12 under G_1 and G_2 ($i = 1, 2, \cdots, 12$)

Table 4 Number of event-triggered instants under different mechanisms with a fixed topology for UAVs 1–12

Mechanism	Number of event-triggered instants												Total	Error ($\times 10^4$)
	1	2	3	4	5	6	7	8	9	10	11	12		
$\lvert\Upsilon_i\rvert$ with θ_1, θ_2	80	316	334	372	487	431	397	499	430	420	439	536	4741	1.1806
$\lvert\Upsilon_i\rvert$ with θ_1	80	315	333	402	506	448	418	530	474	468	492	597	5063	1.2545
Υ_i with θ_1, θ_2	80	315	333	405	511	451	419	537	475	468	491	601	5086	1.2358
Υ_i with θ_1	80	315	333	402	506	448	418	530	474	468	492	597	5063	1.2545

Table 5 Number of event-triggered instants under different mechanisms with a switching topology for UAVs 1–12

Mechanism	Number of event-triggered instants												Total	Error ($\times 10^4$)
	1	2	3	4	5	6	7	8	9	10	11	12		
$\lvert\Upsilon_i\rvert$ with θ_1, θ_2	275	316	602	503	574	555	659	576	525	617	534	540	6276	1.0311
$\lvert\Upsilon_i\rvert$ with θ_1	275	315	593	496	562	548	662	569	522	609	533	537	6221	1.0688
Υ_i with θ_1, θ_2	275	315	595	499	564	549	663	570	522	610	533	537	6232	1.0609
Υ_i with θ_1	275	315	593	496	562	548	662	569	522	609	533	537	6221	1.0670

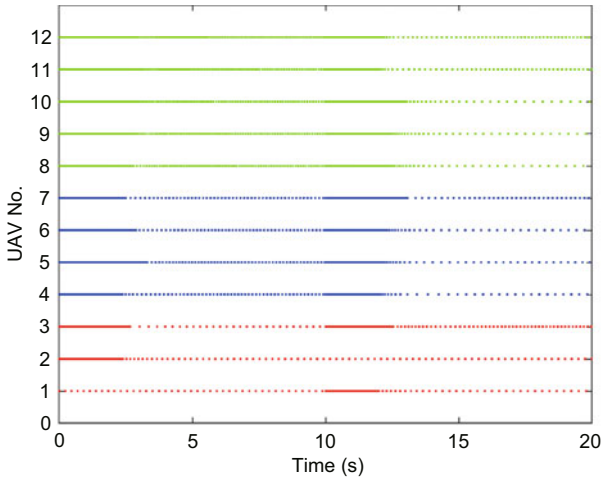

Fig. 12 Triggering instant sequences of UAVs 1–12 under G_1 and G_2

9 Conclusions

In this study, the scaled formation control for MASs subject to fixed and switching topologies is investigated. Different from traditional DET mechanisms, a modified resilient DET mechanism based on sampled data with two different threshold values and the absolute value of the combined error is proposed. A scaled formation control protocol is designed by introducing certain formation information, through which agents in an MAS can realize its formation in groups. Then, by choosing appropriate Lyapunov–Krasovskii functionals (LKFs), the stability of the scaled formation error system is verified. Adoption of the SSA algorithm has made it possible to deploy a co-design algorithm through dealing with the derived criteria in terms of matrix equalities, which is essential for the design of the control gain matrix and triggering parameters. In the end, a multi-UAV system is applied as an example for the confirmation of theoretical results.

It is of significance to explore event-triggered cooperative security control for MASs subject to malicious cyber-attacks. An MAS usually consists of a considerable number of nodes distributed in different spatial locations. The nodes in different regions have different network communication conditions; i.e., the attack type, attack time, and attack intensity may be different. Thus, it is desirable to explore more effective event-triggered security control strategies for MASs in vulnerable networks.

Contributors

Yanping YANG designed the research. Siyu MA drafted the paper. Yanping YANG and Dawei LI helped organize the paper. Dawei LI and Jinghui SUO revised and finalized the paper.

Compliance with ethics guidelines

All the authors declare that they have no conflict of interest.

Data availability

The data that support the findings of this study are available from the corresponding author upon reasonable request.

References

Cao YC, Yu WW, Ren W, et al., 2013. An overview of recent progress in the study of distributed multi-agent coordination. *IEEE Trans Ind Inform*, 9(1):427-438. https://doi.org/10.1109/TII.2012.2219061

Chen WB, Chen YY, Zhang Y, 2022. Finite-time coordinated path-following control of leader-following multi-agent systems. *Front Inform Technol Electron Eng*, 23(10):1511-1521. https://doi.org/10.1631/FITEE.2100476

Dong XW, Zhou Y, Ren Z, et al., 2017. Time-varying formation tracking for second-order multi-agent systems subjected to switching topologies with application to quadrotor formation flying. *IEEE Trans Ind Electron*, 64(6):5014-5024. https://doi.org/10.1109/TIE.2016.2593656

Du SL, Liu T, Ho DWC, 2020. Dynamic event-triggered control for leader-following consensus of multiagent systems. *IEEE Trans Syst Man Cybern Syst*, 50(9):3243-3251. https://doi.org/10.1109/TSMC.2018.2866853

Ge XH, Han QL, Zhang XM, 2018. Achieving cluster formation of multi-agent systems under aperiodic sampling and communication delays. *IEEE Trans Ind Electron*, 65(4):3417-3426. https://doi.org/10.1109/TIE.2017.2752148

Ge XH, Han QL, Zhong MY, et al., 2019. Distributed Krein space-based attack detection over sensor networks under deception attacks. *Automatica*, 109:108557. https://doi.org/10.1016/j.automatica.2019.108557

Ge XH, Xiao SY, Han QL, et al., 2022. Dynamic event-triggered scheduling and platooning control co-design for automated vehicles over vehicular ad-hoc networks. *IEEE/CAA J Autom Sin*, 9(1):31-46. https://doi.org/10.1109/JAS.2021.1004060

Ge XH, Han QL, Wu Q, et al., 2023. Resilient and safe platooning control of connected automated vehicles against intermittent denial-of-service attacks. *IEEE/CAA J Autom Sin*, 10(5):1234-1251. https://doi.org/10.1109/JAS.2022.105845

Guan YP, Ge XH, 2018. Distributed attack detection and secure estimation of networked cyber-physical systems against false data injection attacks and jamming attacks. *IEEE Trans Signal Inform Process Netw*, 4(1):48-59. https://doi.org/10.1109/TSIPN.2017.2749959

Guo XG, Liu PM, Wang JL, et al., 2021. Event-triggered adaptive fault-tolerant pinning control for cluster consensus of heterogeneous nonlinear multi-agent systems under aperiodic DoS attacks. *IEEE Trans Netw Sci Eng*, 8(2):1941-1956. https://doi.org/10.1109/TNSE.2021.3077766

He WL, Mo ZK, 2022. Secure event-triggered consensus control of linear multiagent systems subject to sequential scaling attacks. *IEEE Trans Cybern*, 52(10):10314-10327. https://doi.org/10.1109/TCYB.2021.3070356

He WL, Xu B, Han QL, et al., 2020. Adaptive consensus control of linear multiagent systems with dynamic event-triggered strategies. *IEEE Trans Cybern*, 50(7):2996-3008. https://doi.org/10.1109/TCYB.2019.2920093

He WL, Xu WY, Ge XH, et al., 2022. Secure control of multiagent systems against malicious attacks: a brief survey. *IEEE Trans Ind Inform*, 18(6):3595-3608. https://doi.org/10.1109/TII.2021.3126644

Hu JP, Wu YZ, Li T, et al., 2019. Consensus control of general linear multiagent systems with antagonistic interactions and communication noises. *IEEE Trans Autom Contr*, 64(5):2122-2127. https://doi.org/10.1109/TAC.2018.2872197

Huang J, Wen GG, Peng ZX, et al., 2020. Cluster-delay consensus for second-order nonlinear multi-agent systems. *J Syst Sci Compl*, 33(2):333-344. https://doi.org/10.1007/s11424-020-8174-4

Ju YM, Ding DR, He X, et al., 2022. Consensus control of multi-agent systems using fault-estimation-in-the-loop: dynamic event-triggered case. *IEEE/CAA J Autom Sin*, 9(8):1440-1451. https://doi.org/10.1109/JAS.2021.1004386

Lin ZY, Wang LL, Han ZM, et al., 2014. Distributed formation control of multi-agent systems using complex Laplacian. *IEEE Trans Autom Contr*, 59(7):1765-1777. https://doi.org/10.1109/TAC.2014.2309031

Luo SP, Ye D, 2022. Cluster consensus control of linear multiagent systems under directed topology with general partition. *IEEE Trans Autom Contr*, 67(4):1929-1936. https://doi.org/10.1109/TAC.2021.3069398

Ma L, Wang YL, Han QL, 2021. H_∞ cluster formation control of networked multiagent systems with stochastic sampling. *IEEE Trans Cybern*, 51(12):5761-5772. https://doi.org/10.1109/TCYB.2019.2959201

Mahony R, Kumar V, Corke P, 2012. Multirotor aerial vehicles: modeling, estimation, and control of quadrotor. *IEEE Robot Autom Mag*, 19(3):20-32. https://doi.org/10.1109/MRA.2012.2206474

Meng DY, Jia YM, 2016. Scaled consensus problems on switching networks. *IEEE Trans Autom Contr*, 61(6):1664-1669. https://doi.org/10.1109/TAC.2015.2479119

Ning BD, Han QL, Zuo ZY, et al., 2023. Fixed-time and prescribed-time consensus control of multiagent systems and its applications: a survey of recent trends and methodologies. *IEEE Trans Ind Inform*, 19(2):1121-1135. https://doi.org/10.1109/TII.2022.3201589

Park P, Ko JW, Jeong C, 2011. Reciprocally convex approach to stability of systems with time-varying delays. *Automatica*, 47(1):235-238. https://doi.org/10.1016/j.automatica.2010.10.014

Ren W, Atkins E, 2005. Second-order consensus protocols in multiple vehicle systems with local interactions. Proc AIAA Guidance, Navigation, and Control Conf and Exhibit. https://doi.org/10.2514/6.2005-6238

Roy S, 2015. Scaled consensus. *Automatica*, 51:259-262. https://doi.org/10.1016/j.automatica.2014.10.073

Shan YH, Hu JF, Chan KW, et al., 2021. A unified model predictive voltage and current control for microgrids with distributed fuzzy cooperative secondary control. *IEEE Trans Ind Inform*, 17(12):8024-8034. https://doi.org/10.1109/TII.2021.3063282

Shen B, Wang ZD, Wang D, et al., 2020. Distributed state-saturated recursive filtering over sensor networks under round-robin protocol. *IEEE Trans Cybern*, 50(8):3605-3615. https://doi.org/10.1109/TCYB.2019.2932460

Su YF, Cai H, Huang J, 2022. The cooperative output regulation by the distributed observer approach. *Int J Netw Dynam Intell*, 1(1):20-35. https://doi.org/10.53941/ijndi0101003

Wang H, Yu WW, Wen GH, et al., 2019. Fixed-time consensus of nonlinear multi-agent systems with general directed topologies. *IEEE Trans Circ Syst II Expr Briefs*, 66(9):1587-1591. https://doi.org/10.1109/TCSII.2018.2886298

Wang JH, Bao F, Han L, et al., 2020. Discrete sliding mode control for time-varying formation tracking of multi-UAV system with a dynamic leader. Proc Chinese Automation Congress, p.4950-4955. https://doi.org/10.1109/CAC51589.2020.9327623

Wang XL, Sun Y, Ding DR, 2022. Adaptive dynamic programming for networked control systems under communication constraints: a survey of trends and techniques. *Int J Netw Dynam Intell*, 1(1):85-98. https://doi.org/10.53941/ijndi0101008

Xie ML, Ding DR, Ge XH, et al., 2023. Distributed platooning control of automated vehicles subject to replay attacks based on proportional integral observers. *IEEE/CAA J Autom Sin*, early access. https://doi.org/10.1109/JAS.2022.105941

Xu B, He WL, 2018. Event-triggered cluster consensus of leader-following linear multi-agent systems. *J Artif Intell Soft Comput Res*, 8(4):293-302. https://doi.org/10.1515/jaiscr-2018-0019

Xue JK, Shen B, 2020. A novel swarm intelligence optimization approach: sparrow search algorithm. *Syst Sci Contr Eng*, 8(1):22-34. https://doi.org/10.1080/21642583.2019.1708830

Ye MJ, Han QL, Ding L, et al., 2023. Distributed Nash equilibrium seeking in games with partial decision information: a survey. *Proc IEEE*, 111(2):140-157. https://doi.org/10.1109/JPROC.2023.3234687

Ye N, Zhang YB, Borror CM, 2004. Robustness of the Markov-chain model for cyber-attack detection. *IEEE Trans Rel*, 53(1):116-123. https://doi.org/10.1109/TR.2004.823851

Yu JJ, Zhang KJ, Fei SM, 2009. Further results on mean square exponential stability of uncertain stochastic delayed neural networks. *Commun Nonl Sci Numer Simul*, 14(4):1582-1589. https://doi.org/10.1016/j.cnsns.2008.04.009

Yu JL, Dong XW, Li QD, et al., 2022. Adaptive practical optimal time-varying formation tracking control for disturbed high-order multi-agent systems. *IEEE Trans Circ Syst I Reg Papers*, 69(6):2567-2578. https://doi.org/10.1109/TCSI.2022.3151464

Zhang D, Xu ZH, Karimi HR, et al., 2018. Distributed H_∞ output-feedback control for consensus of heterogeneous linear multiagent systems with aperiodic sampled-data communications. *IEEE Trans Ind Electron*, 65(5):4145-4155. https://doi.org/10.1109/TIE.2017.2772196

Zhang LZ, Li YY, Lou JG, et al., 2022. Bipartite asynchronous impulsive tracking consensus for multi-agent systems. *Front Inform Technol Electron Eng*, 23(10):1522-1532. https://doi.org/10.1631/FITEE.2100122

Zhang XM, Han QL, Ge XH, et al., 2023. Sampled-data control systems with non-uniform sampling: a survey of methods and trends. *Ann Rev Contr*, 55:70-91. https://doi.org/10.1016/j.arcontrol.2023.03.004

Zhu GL, Liu KX, Gu HB, et al., 2022. Observer-based event-triggered formation control of multi-agent systems with switching directed topologies. *IEEE Trans Circ Syst I Reg Papers*, 69(3):1323-1332. https://doi.org/10.1109/TCSI.2021.3134816

Appendix A: Proof of Theorem 1

The following Lyapunov–Krasovskii functionals (LKFs) are chosen:

$$\begin{aligned}\mathcal{V}(t)=&\sum_{i=1}^{N}\eta_i(t)+z^{\mathrm{T}}(t)(U\otimes R_1)z(t)\\&+\sum_{i=1}^{N}\int_{t-\bar{\tau}_i}^{t}z^{\mathrm{T}}(s)(U\otimes R_2)z(s)\mathrm{d}s\\&+\sum_{i=1}^{N}\bar{\tau}_i\int_{-\bar{\tau}_i}^{0}\int_{t+\theta}^{t}\dot{z}^{\mathrm{T}}(s)(U\otimes R_3)\dot{z}(s)\mathrm{d}s\mathrm{d}\theta\\&+\sum_{i=1}^{N}\Big(\bar{\tau}_i^2\int_{t_k+\ell h}^{t}\dot{z}^{\mathrm{T}}(s)(U\otimes R_4)\dot{z}(s)\mathrm{d}s\\&-\frac{\pi^2}{4}\int_{t_k+\ell h}^{t}\big(z(s)-z(t_k+\ell h)\big)^{\mathrm{T}}(U\otimes R_4)\\&\cdot\big(z(s)-z(t_k+\ell h)\big)\mathrm{d}s\Big),\end{aligned}\tag{A1}$$

where $U=L+L^{\mathrm{T}}>0$, $R_\epsilon>0$ ($\epsilon=1,2,3,4$).

Taking the derivative of LKF (A1) yields

$$\begin{aligned}&\dot{\mathcal{V}}(t)\\&=\sum_{i=1}^{N}\dot{\eta}_i(t)+2z^{\mathrm{T}}(t)(U\otimes R_1)\dot{z}(t)+z^{\mathrm{T}}(t)(U\otimes R_2)z(t)\\&\quad-\sum_{i=1}^{N}z^{\mathrm{T}}(t-\bar{\tau}_i)(U\otimes R_2)z(t-\bar{\tau}_i)\\&\quad+\sum_{i=1}^{N}\bar{\tau}_i{}^2\dot{z}^{\mathrm{T}}(t)(U\otimes R_3)\dot{z}(t)\\&\quad-\sum_{i=1}^{N}\bar{\tau}_i\int_{t-\bar{\tau}_i}^{t}\dot{z}^{\mathrm{T}}(s)(U\otimes R_3)\dot{z}(s)\mathrm{d}s\\&\quad+\sum_{i=1}^{N}\Big(\bar{\tau}_i^2\dot{z}^{\mathrm{T}}(t)(U\otimes R_4)\dot{z}(t)-\frac{\pi^2}{4}\big(z(t)\\&\quad-z(t-\tau_i(t))\big)^{\mathrm{T}}(U\otimes R_4)\big(z(t)-z(t-\tau_i(t))\big)\Big).\end{aligned}\tag{A2}$$

By applying a reciprocally convex approach (Park et al., 2011), one obtains

$$\sum_{i=1}^{N}\bar{\tau}_i\int_{t-\bar{\tau}_i}^{t}\dot{z}^{\mathrm{T}}(s)(U\otimes R_3)\dot{z}(s)\mathrm{d}s\geq\eta^{\mathrm{T}}(t)\Xi\eta(t),$$

where $\eta(t)=\mathrm{col}\{z(t)-z(t-\tau_i(t)),\ z(t-\tau_i(t))-z(t-\bar{\tau}_i)\}$.

According to the modified DET mechanism (4), the following inequality can be ensured:

$$\begin{aligned}
&\sum_{i=1}^{N}\dot{\zeta}_i(t)\\
=&\sum_{i=1}^{N}(-\beta_i\zeta_i(t)+\big(\kappa_{\hat{i}}\theta_1+(1-\kappa_{\hat{i}})\theta_2\big)\mathrm{sgn}[\Upsilon_i]\Upsilon_i)\\
\leq&\sum_{i=1}^{N}\mathrm{sgn}[\Upsilon_i](\tilde{\theta}-\beta_i)\delta_i(e^{\mathrm{T}}(t-\tau_i(t))\Phi e(t-\tau_i(t))\\
&-\sigma_i z^{\mathrm{T}}(t-\tau_i(t))(HL^iH^{-1}\otimes I_N)^{\mathrm{T}}\Omega(HL^iH^{-1}\otimes I_N)\\
&\cdot z(t-\tau_i(t))+\sigma_i z^{\mathrm{T}}(t-\tau_i(t))(HL^iH^{-1}\otimes I_N)^{\mathrm{T}}\Omega\\
&\cdot(HL^i\alpha^{-1}\otimes I_N)f(t-\tau_i(t))+\sigma_i f^{\mathrm{T}}(t-\tau_i(t))\\
&\cdot(HL^i\alpha^{-1}\otimes I_N)^{\mathrm{T}}\Omega(HL^iH^{-1}\otimes I_N)z(t-\tau_i(t))\\
&-\sigma_i f^{\mathrm{T}}(t-\tau_i(t))(HL^i\alpha^{-1}\otimes I_N)^{\mathrm{T}}\Omega(HL^i\alpha^{-1}\otimes I_N)\\
&\cdot f(t-\tau_i(t))).
\end{aligned}\tag{A3}$$

Let $\varphi(t)=\mathrm{col}\{z(t),z(t-\tau(t)),z(t-\bar{\tau}),f(t-\tau(t)),e(t-\tau(t))\}$, where $z(t-\tau(t))=\mathrm{col}\{z(t-\tau_1(t)),\cdots,z(t-\tau_N(t))\}$, $z(t-\bar{\tau})=\mathrm{col}\{z(t-\bar{\tau}_1),\cdots,z(t-\bar{\tau}_N)\}$, $f(t-\tau(t))=\mathrm{col}\{f(t-\tau_1(t)),\cdots,f(t-\tau_N(t))\}$, $e(t-\tau(t))=\mathrm{col}\{e(t-\tau_1(t)),\cdots,e(t-\tau_N(t))\}$. Then the following inequality is obtained:

$$\dot{\mathcal{V}}(t)\leq\varphi^{\mathrm{T}}(t)\Gamma\varphi(t).\tag{A4}$$

$\dot{\mathcal{V}}(t)<0$ can be inferred from inequality (15).

Appendix B: Proof of Theorem 2

Appropriate LKFs are chosen as

$$\begin{aligned}
&\mathcal{V}(t)\\
=&\sum_{i=1}^{N}\eta_i(t)+z^{\mathrm{T}}(t)(U\otimes R_1^b)z(t)\\
&+\sum_{i=1}^{N}\int_{t-\bar{\tau}_i}^{t}z^{\mathrm{T}}(s)(U\otimes R_2)z(s)\mathrm{d}s\\
&+\sum_{i=1}^{N}\bar{\tau}_i\int_{-\bar{\tau}_i}^{0}\int_{t+\theta}^{t}z^{\mathrm{T}}(s)(U\otimes R_3)z(s)\mathrm{d}s\mathrm{d}\theta\\
&+\sum_{i=1}^{N}\Big(\bar{\tau}_i^2\int_{t_k+\ell h}^{t}z^{\mathrm{T}}(s)(U\otimes R_4)z(s)\mathrm{d}s\\
&-\frac{\pi^2}{4}\int_{t_k+\ell h}^{t}\big(z(s)-z(t_k+\ell h)\big)^{\mathrm{T}}(U\otimes R_4)\\
&\cdot\big(z(s)-z(t_k+\ell h)\big)\mathrm{d}s\Big),
\end{aligned}\tag{B1}$$

where $R_1^b>0$, $R_\epsilon>0$, $\epsilon=1,2,3,4$.

We define the weak infinitesimal operator $\mathcal{L}$ of $\mathcal{V}(t)$ as

$$\mathcal{L}\mathcal{V}(t)=\sup\lim_{\triangle t\to 0}\frac{\mathbb{E}\{\mathcal{V}(t+\triangle t)-\mathcal{V}(t)\}}{\triangle t}.$$

Then one can obtain

$$\begin{aligned}
&\mathcal{L}\mathcal{V}(t)\\
=&\sum_{i=1}^{N}\dot{\zeta}_i(t)+2\sum_{q=1}^{r}z^{\mathrm{T}}(t)(U\otimes(\xi_{pq}R_1^b))\dot{z}(t)\\
&+z^{\mathrm{T}}(t)(U\otimes R_2)z(t)\\
&-\sum_{i=1}^{N}z^{\mathrm{T}}(t-\bar{\tau}_i)(U\otimes R_2)z(t-\bar{\tau}_i)\\
&+\sum_{i=1}^{N}\bar{\tau}_i{}^2\dot{z}^{\mathrm{T}}(t)(U\otimes R_3)\dot{z}(t)\\
&-\sum_{i=1}^{N}\bar{\tau}_i\int_{t-\bar{\tau}_i}^{t}\dot{z}^{\mathrm{T}}(s)(U\otimes R_3)\dot{z}(s)\mathrm{d}s\\
&+\sum_{i=1}^{N}\Big(\bar{\tau}_i^2\dot{z}^{\mathrm{T}}(t)(U\otimes R_4)\dot{z}(t)-\frac{\pi^2}{4}\big(z(t)\\
&-z(t-\tau_i(t))\big)^{\mathrm{T}}(U\otimes R_4)\big(z(t)-z(t-\tau_i(t))\big)\Big).
\end{aligned}\tag{B2}$$

By applying a reciprocally convex approach (Park et al., 2011), one can obtain

$$\begin{aligned}
&\mathbb{E}\Big\{\sum_{i=1}^{N}\bar{\tau}_i\int_{t-\bar{\tau}_i}^{t}\dot{z}^{\mathrm{T}}(s)(U\otimes R_3)\dot{z}(s)\mathrm{d}s\Big\}\\
&\qquad\geq\mathbb{E}\Big\{\eta^{\mathrm{T}}(t)\Xi\eta(t)\Big\}.
\end{aligned}$$

According to the modified resilient DET mechanism (4), the following inequality is ensured:

$$\begin{aligned}
&\mathcal{L}\sum_{i=1}^{N}\zeta_i(t)=\sum_{i=1}^{N}(-\beta_i\zeta_i(t)+\big(\kappa_{\hat{i}}\theta_1+(1-\kappa_{\hat{i}})\theta_2\big)\mathrm{sgn}[\Upsilon_i]\Upsilon_i)\\
&\leq\sum_{i=1}^{N}\mathrm{sgn}[\Upsilon_i](\tilde{\theta}-\beta_i)\delta_i(e^{\mathrm{T}}(t-\tau_i(t))\Phi e(t-\tau_i(t))\\
&-\sigma_i z^{\mathrm{T}}(t-\tau_i(t))(HL_b^iH^{-1}\otimes I_N)^{\mathrm{T}}\Omega(HL_b^iH^{-1}\otimes I_N)
\end{aligned}$$

$$\cdot z(t-\tau_i(t))+\sigma_i z^{\mathrm{T}}(t-\tau_i(t))(HL_b^iH^{-1}\otimes I_N)^{\mathrm{T}}\Omega$$
$$\cdot(HL_b^i\alpha_b^{-1}\otimes I_N)f(t-\tau_i(t))+\sigma_i f^{\mathrm{T}}(t-\tau_i(t))$$
$$\cdot(HL_b^i\alpha_b^{-1}\otimes I_N)^{\mathrm{T}}\Omega(HL_b^iH^{-1}\otimes I_N)z(t-\tau_i(t))$$
$$-\sigma_i f^{\mathrm{T}}(t-\tau_i(t))(HL_b^i\alpha_b^{-1}\otimes I_N)^{\mathrm{T}}\Omega(HL_b^i\alpha_b^{-1}\otimes I_N)$$
$$\cdot f(t-\tau_i(t))). \tag{B3}$$

Let $\varphi(t)=\mathrm{col}\{z(t),z(t-\tau(t)),z(t-\bar{\tau}),f(t-\tau(t)),e(t-\tau(t))\}$. Then, we can obtain

$$\mathbb{E}\{\mathcal{L}\mathcal{V}(t)\}\le\mathbb{E}\{\varphi^{\mathrm{T}}(t)\Psi\varphi(t)\}. \tag{B4}$$

In view of inequality (B4), there exists a scalar ϖ such that

$$\mathbb{E}\{\mathcal{L}\mathcal{V}(t)\}\le-\varpi\mathbb{E}\{\|z(t)\|^2\}.$$

We define $\hat{\mathcal{V}}(t)=\mathrm{e}^{\nu t}$, $\nu>0$; then, we have

$$\mathcal{L}\hat{\mathcal{V}}(t)=\mathrm{e}^{\nu t}[\nu\mathcal{V}(t)+\mathcal{L}\mathcal{V}(t)]. \tag{B5}$$

For Eq. (B5), we apply the integral from 0 to $T>0$ on both sides, and calculate expectation

$$\mathbb{E}\{\mathrm{e}^{\nu t}\mathcal{V}(T)\}-\mathbb{E}\{\mathcal{V}(0)\}$$
$$=\int_0^{\mathrm{T}}\nu\mathrm{e}^{\nu t}\mathbb{E}\{\mathcal{V}(t)\}\mathrm{d}t+\int_0^T\mathrm{e}^{\nu t}\mathbb{E}\{\mathcal{L}\mathcal{V}(t)\}\mathrm{d}t.$$

Thus, there exists a scalar $\varpi>0$ such that

$$\mathbb{E}\{\mathcal{V}(T)\}\le\varpi\mathrm{e}^{-\nu t}\sup_{-\bar{\tau}\le\theta\le0}\mathbb{E}\{\|\psi(\theta)\|^2\}.$$

As $\mathcal{V}(T)\ge\varrho z^{\mathrm{T}}(T)z(T)$, where $\varrho=\min_{b=1,2,\cdots,r}\{\lambda_{\min}(R_1^b)\}$, it holds that

$$\mathbb{E}\{\|z(T)\|^2\}\le\frac{\varpi}{\varrho}\mathrm{e}^{-\nu t}\sup_{-\bar{\tau}\le\theta\le0}\mathbb{E}\{\|\psi(\theta)\|^2\}. \tag{B6}$$